UCRL-ID-112719

PCMDI
Program for Climate Model Diagnosis and Intercomparison

PCMDI Report No. 8

THE IMPACT OF HORIZONTAL RESOLUTION ON MOIST PROCESSES IN THE ECMWF MODEL

by

Thomas J. Phillips, Lisa C. Corsetti and Stanley L. Grotch

Program for Climate Model Diagnosis and Intercomparison
Lawrence Livermore National Laboratory, Livermore, CA, USA

January 1993

PROGRAM FOR CLIMATE MODEL DIAGNOSIS AND INTERCOMPARISON
UNIVERSITY OF CALIFORNIA, LAWRENCE LIVERMORE NATIONAL LABORATORY
LIVERMORE, CA 94550

ABSTRACT

Summer and winter climates simulated at spectral scales T21, T42, T63 and T106 with the ECMWF (cycle 33) model are analyzed to determine the impact of changes in horizontal resolution (in the absence of changes in model physics) on atmospheric water vapor, clouds, convection, and precipitation. Qualitative changes in many moist processes occur in the transition from spectral T21 to T42, especially in the tropics where atmospheric convection plays a central role; subsequent resolution increases mostly result in an intensification of patterns established at T42.

However, the seasonal climate simulations do not show evidence of "convergence" to an asymptotic climate state at high resolution. Global convective precipitation increases monotonically with resolution, but frontal precipitation, precipitable water, and cloud cover display a qualitatively different pattern; after undergoing abrupt reductions in the transition from T21 to T42, their global averages show relative increases at finer resolutions. Precipitable water and cloud cover also display a seasonal asymmetry in their responses to increasing resolution.The comparative insensitivity of global cloud cover to resolution is mainly a consequence of compensating tendencies of clouds in different regions. With increasing resolution, decreases in low-latitude clouds that result from drying of the tropical atmosphere are partially offset by increases in high-latitude clouds associated with enhanced relative humidity in response to an intensifying extratropical cold bias.

The large-scale tropical moist processes are modeled more realistically at T21 than in the finer-resolution simulations, wherein anomalous seasonal climatic features such as a double ITCZ and underdeveloped summer monsoon circulation are evident. Although some of these anomalies might ameliorate if the physical parameterizations were suitably "tuned," these deficiencies may reflect more fundamental problems related to a mismatch between the resolution of the model and the implicit spatial and temporal scales of the parameterizations.

1. Introduction

The impact of horizontal resolution on simulations of atmospheric dynamics by general circulation models (GCMs) has been of long-term interest (e.g., Manabe et al. 1970, Wellck et al. 1971), and these issues are being investigated anew for the current generation of models (e.g., Boer and Lazare 1988, Boville 1991). In contrast, the resolution-dependence of the moist processes simulated by GCMs has received only comparatively recent attention--chiefly by Rind (1988), Tibaldi et al. (1990), Kiehl and Williamson (1991), and Morcrette (1991).

From analyses of warm-climate simulations with 4x5-degree and 8x10-degree versions of the Goddard Institute for Space Studies (GISS) model, Rind (1988) found that cloud cover decreased with increasing resolution. The greatest impact was felt by the simulated high-level clouds, owing to the combined effects of the cloud formation scheme and the warmer upper-tropospheric temperatures associated with greater penetrative convection in the higher-resolution model. Enhanced global-average precipitation also attended the increase in resolution.

Although primarily concerned with the impact of resolution on extended-range forecasting of dynamical fields in the ECMWF (cycle 28) model, Tibaldi et al. (1990) also analyzed the resolution-dependence of some moist processes. The authors inferred that convective heating driving the modeled Asian summer monsoon was simulated with progressively less realism as resolution increased from T21 to T106, and attributed this to the noisier high-resolution convergence of moisture that provided closure for the modified Kuo (1974) convective scheme then in use in the ECMWF model. They noted, however, that realistic simulation of orographic monsoon rainfall demanded a resolution finer than T21.

In diagnosing January climate simulations with the NCAR Community Climate Model (CCM1), Kiehl and Williamson (1991) reported a large and monotonic decrease in cloud cover as resolution increased from spectral T21 to T106. In contrast to Rind's results, the greatest impact of the resolution change was felt by the low-level clouds as a consequence of the enhanced subsidence and drying of the lower troposphere that accompanied the resolution increase. Global precipitation increased with resolution.

Morcrette (1991), however, found that the global cloud cover simulated for July by the ECMWF (cycle 36) model was much less sensitive to resolution than that in the NCAR model. He also noted that global cloud cover was fairly insensitive to major

changes in the model's convection scheme.

The present study focuses on the effects of resolution on precipitation, atmospheric moisture, and clouds in the ECMWF (cycle 33) model. The cited previous analyses of this kind suggest that the relationship between resolution and the simulated moist processes is complex, and that model-specific anomalies cannot yet be unambiguously separated from ubiquitous phenomena. Diagnosis of the simulation of the moisture fields is complicated by the interplay of dynamics approximated at the scale of the model grid and physics that operates either through gridscale variables (e.g., atmospheric moisture) or through parameterized subgridscale processes (e.g., convection). The present study of resolution effects on the moist variables therefore is intended as another contribution to an ongoing sorting-out process for GCMs; this can proceed further for the ECMWF (cycle 33) model because the parallel studies by Morcrette (1991) and Tibaldi et al. (1990) analyze other versions of the ECMWF model with somewhat different physics. Secondary goals of this study are to assess whether the model's moist processes are better simulated at a particular resolution, insofar as this can be ascertained from available observational data, and whether the simulated seasonal climates show evidence of "convergence" as the horizontal resolution increases.

The present study is part of a comprehensive diagnosis of the resolution-dependence of the ECMWF (cycle 33) model that has been undertaken by the Program for Climate Model Diagnosis and Intercomparison (PCMDI). To date, other papers in this series include detailed analyses of the impact of resolution on model dynamics (Boyle 1993), on ocean surface energy fluxes (Gleckler and Taylor 1993), and on the intraseasonal variability of the simulated summer monsoon circulation over India (Sperber 1993) and over China (Potter et al. 1993).

The features of the ECMWF model most relevant to an investigation of moist processes are described in Section 2, where the resolution experiments also are briefly summarized. The results of the study are elaborated in Section 3, and conclusions are drawn in Section 4.

2. The ECMWF model and the resolution experiments

a. *Model description*

The ECMWF atmospheric general circulation model is based on the primitive

equations expressed in spectral form, and many physical processes of importance for climate simulation also are included (cf. ECMWF Research Department 1988a,b; Simmons et al. 1989). The ECMWF (cycle 33) model used for the present study differs in several respects from the cycle 28 version that was diagnosed by Tibaldi et al. (1990) and from cycle 36, which was the focus of the Morcrette (1991) study. Major differences from cycle 28 include new parameterizations of atmospheric radiation (Morcrette 1989), gravity-wave drag (Miller et al. 1989), land surface processes (Blondin and Böttger 1987), and the removal of vertical diffusion above the planetary boundary layer. The vertical resolution of cycle 33 also is finer than that in cycle 28 (19 versus 16 vertical levels). Perhaps most relevant for the present study, subgrid-scale deep convection in cycle 33 is represented by the mass-flux parameterization of Tiedtke (1989), whereas a modified Kuo (1974) scheme was used in cycle 28.

In the Tiedtke (1989) formulation shallow, mid-level, and penetrative convection are accounted for, and the effects of cumulus-scale downdrafts are included. For mid-level and penetrative convection, the closure assumption is that large-scale moisture convergence determines the bulk cloud mass flux; for shallow convection, however, the mass flux is maintained instead by moisture from surface evaporation through an extended version of the model's vertical diffusion scheme. Freezing and melting processes in convective clouds are not considered, and the conversion from cloud droplets to raindrops is proportional to the cloud liquid water content. Entrainment of mass at the bases of convective plumes and detrainment at their tops occur both through turbulent exchange at the cloud edges and through organized inflow associated with large-scale convergence. If cloud liquid water is detrained into the environment, it is assumed to evaporate instantaneously there. The portion of this liquid water that does not moisten the environment falls out of the cloud as convective precipitation. This precipitate can change to snow below the cloud only if the near-surface air temperature is less than -3 C, and over land only if the surface temperature is below 0 C. The precipitation at the surface is equal to the amount falling from the cloud minus that which evaporates between the cloud base and the ground. Evaporation of convective precipitation is parameterized as a function of the convective rain intensity and of the difference between saturated specific humidity and that of the environment.

Other moist processes are represented similarly in cycles 28 and 33 of the model. Precipitation from condensation is simulated explicitly at the scale of the horizontal and vertical grid. Such gridscale precipitation is produced when the specific humidity

exceeds the saturated value at the given temperature and pressure, the amount of precipitate depending on the new equilibrium value of specific humidity resulting from the accompanying release of latent heat. Precipitation may fall as snow if the temperature of the layer where condensation occurs is below 0 C. Evaporation of grid-scale precipitation is modeled by demanding that it must saturate a layer before being allowed to fall to the next layer below.

In both ECMWF cycles 28 and 33 clouds are diagnostically determined after the method of Slingo (1987). These are of three types: clouds associated with shallow (stratocumulus), mid-level (cumulus), or penetrative (cumulonimbus) convection; clouds produced by midlatitude fronts and tropical disturbances that form in low (stratus), middle (altostratus, altocumulus), or high (cirrus) vertical layers; and stratus clouds that are associated with temperature inversions in the lowest model layers. Due to the model's inability to realistically simulate fog formation and dissipation, no cloud is allowed to form in the lowest vertical layer. The total top-of-atmosphere cloud cover is computed assuming random overlap of clouds of different types in different layers, but assuming full overlap of convective clouds and of gridscale clouds of the same type in adjacent layers.

In the ECMWF (cycle 33) model convective clouds may occupy any number of vertical layers, the base of the cloud being at the lowest level of moist convective instability and the cloud top at the level of non-buoyancy for moist adiabatic ascent of an air parcel. Nonprecipitating convective cloud amount is limited to 20% of a grid square, while precipitating convective cloud amount is scaled proportional to the logarithm of the time-average precipitation rate up to a maximum of 80% of a grid square. If cumulo-nimbus clouds penetrate above 400 hPa and cover at least 40% of a grid square, anvil cirrus clouds also form. In such cases only 25% of the predicted cloud amount is allowed to occupy the full depth, the remaining 75% being treated as shallow convective cloud in accordance with the observation that cumulonimbus clouds usually coexist with larger amounts of lower-level cloud.

High, middle, and low gridscale clouds associated with fronts and tropical disturbances form when the relative humidity is greater than a threshold of 80%, the cloud amount being a function of this excess humidity. In addition, the amount of this middle and low cloud is reduced in the presence of dry convective downdrafts. Low cloud forms in subsiding air only where there is a temperature inversion with the relative humidity at the base of the inversion exceeding 60%. For conditions of weak ascent

(pressure tendency between -0.1 and 0.0 Pa s^{-1}) the amount of low cloud is scaled proportionally to the magnitude of the pressure tendency. Under subsident conditions low cloud amount depends on the strength of the temperature inversion and the relative humidity excess above 60%.

There also are a few differences between the ECMWF (cycle 33) model and the cycle 36 version diagnosed by Morcrette (1991) that are relevant for the simulation of moist processes. First, changes made to the moisture and heat transfer coefficients over the oceans in cycle 36 produce substantially higher (and probably more realistic) latent heat fluxes in regions where calm surface winds prevail (Miller et al., 1992). Second, whereas in cycles 28 and 33 the amount of nonprecipitating convective cloud cannot exceed 20% of a grid square, in cycle 36 the amount of this type of cloud is determined from the condensation rate--the difference between the moisture flux at cloud base and that detrained at cloud top. This change produces larger amounts of shallow convective cloud than in cycle 33, especially in the marine trade wind zones. In other respects, however, the ECMWF (cycle 36) model includes the same Tiedtke (1989) formulation of convection as in the cycle 33 version.

b. The resolution experiments

After being initialized from the ECMWF observational analysis for 1 January 1987, the model was integrated with temporally varying solar forcing, and with sea surface temperatures and ice extents prescribed from the monthly climatology of Alexander and Mobley (1976), where daily updates were computed by linear interpolation. The model was run for a total of 15 months at spectral T21, T63, and T106 resolutions (roughly equivalent to grid spacings of 5.6x5.6, 1.9x1.9, and 1.1x1.1 deg, respectively--cf. Laprise 1992), and for a total of 24 months at spectral T42 resolution (equivalent grid spacing 2.8x2.8 deg). The coefficients for biharmonic (∇^4) horizontal diffusion at T106 were set to half the values used in the T21-T63 versions, a practice followed in the resolution experiments of Tibaldi et al. (1990). No other modifications were made to the model as resolution was increased from T21 to T106.

At each resolution monthly-averaged fields were computed either from samples at six-hour intervals or, in the case of precipitation and runoff, from daily accumulations. Seasonal averages were then computed, with the Northern Hemisphere winter statistics being determined from the simulation of December and the second January

and February in the histories for each resolution. In addition, the differences between year 1 and 2 of the T42 simulation provided rough estimates of the interannual variability of the simulated seasonal climates.

3. Resolution-dependence of precipitation, humidity, and cloudiness

In diagnosing the effects of resolution on the model's moist processes, we consider impacts on precipitation and clouds, distinguishing between the convective and nonconvective portions of these elements. These effects, in turn, are related to corresponding resolution-dependent changes in atmospheric moisture.

We focus attention on June-July-August (JJA) and December-January-February (DJF) averages because convection is most vigorous in these extreme seasons and its impact on all the moist processes is most dramatic. We also emphasize only those resolution-dependent changes that are larger than the interannual variability of the model, as estimated from the T42 simulation. For consistent comparison across different resolutions, results are projected onto a common T21 Gaussian grid by means of an equal-area weighting interpolation algorithm.

a. Precipitation

Total precipitation

The JJA seasonal-average of the gauge-corrected observational precipitation dataset of Legates and Willmott (1990) is shown in Fig. 1a. By far the heaviest precipitation (> 12 mm day^{-1}) falls in the tropics, with substantially lower values (2-6 mm day^{-1}) at other latitudes. Differences between simulated and observed precipitation at the respective resolutions shown in Figs. 1b-d are largest in the tropics. Some of these, such as the negative departures near 150 W in the equatorial Pacific, probably are not indicative of a model deficiency, since here the Legates-Willmott data differ substantially from other precipitation estimates (Janowiak 1992). Other systematic differences, such as the simulation of excessive precipitation at high southern latitudes, occur in observation-sparse regions. However, where the observational data are more reliable (such as over land) the model appears to be generally too dry.

Especially in the tropics, the pattern of precipitation departures at T21 (Fig. 1b)

is qualitatively different from those at T42-T106 resolutions (Fig. 1c-e). The T21 simulation is in better agreement with observations in the equatorial West Pacific and to the north of Australia, where the extensive positive precipitation discrepancy at T42-T106 is associated with a spurious double ITCZ that is present in JJA.

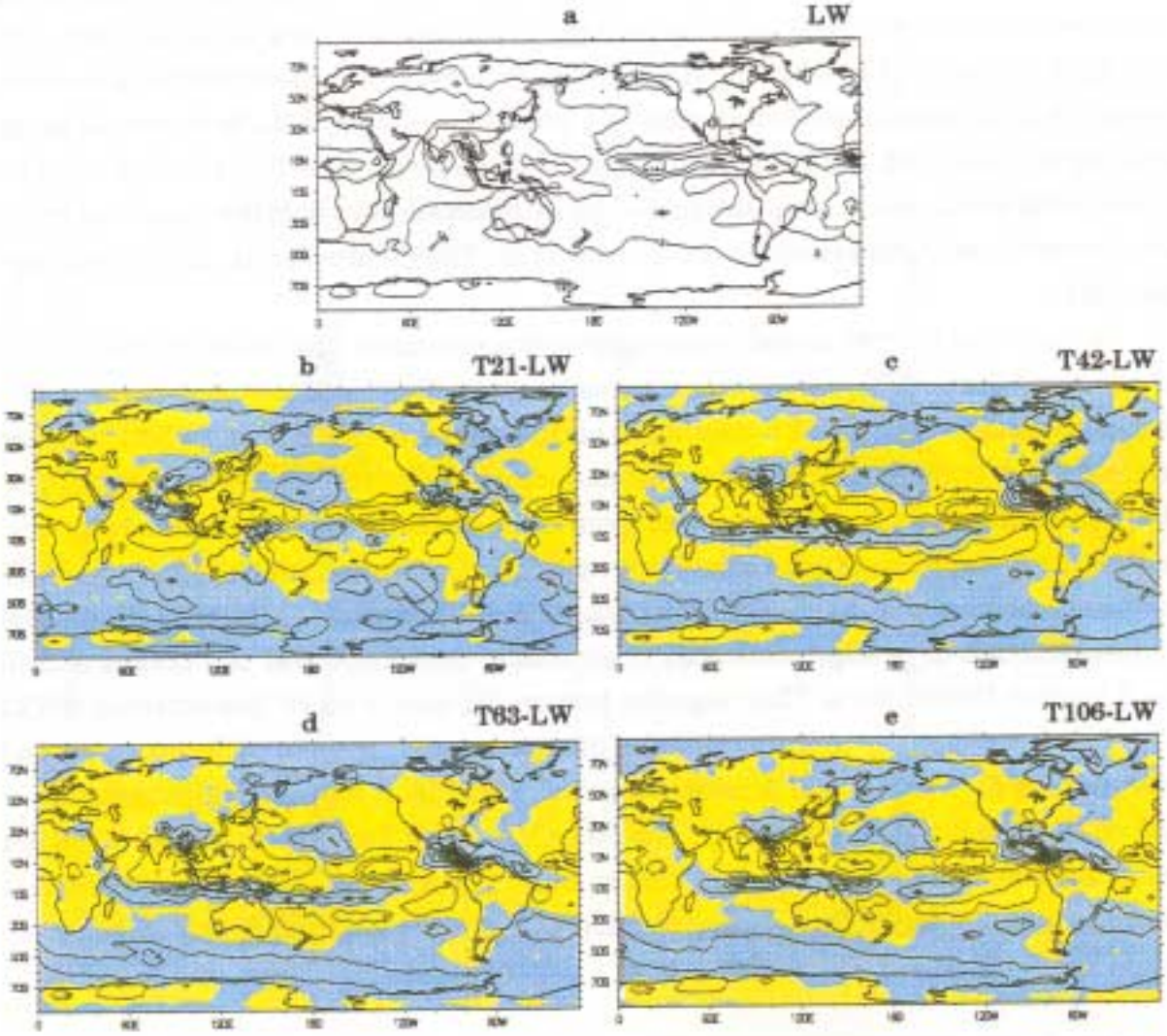

Fig. 1. JJA precipitation (in mm day^{-1}) from the gauge-corrected Legates-Willmott (LW) observational rainfall data (a, with contours starting at 2 mm day^{-1} and spaced at 4 mm day^{-1} intervals), and departures from this at resolutions T21 (b), T42 (c), T63 (d), and T106 (e). Areas drier than the observations are shaded yellow, while wetter areas are shaded blue. Difference contours start at ± 2 mm day^{-1} and are spaced at ± 4 mm day^{-1} intervals.

Qualitative differences occur in the Asian monsoon region as well: At the higher resolutions precipitation over the Indian and Indonesian sectors is too scant by as much as 10 mm day^{-1}, while here it is somewhat too abundant in the T21 simulation. At T42-T106 the model also produces too much precipitation near Central America that is associated with an overly intense convection center (Boyle 1993). Finally, the excessive simulation of precipitation at high southern latitudes is more marked at T42-T106 than at T21 resolution. Thus, although substantial precipitation discrepancies occur at all resolutions in JJA, the T21 simulation displays the best overall large-scale agreement with the Legates-Willmott observations. (The T21 simulation of regional-scale monsoonal precipitation and its intraseasonal variability compares much less favorably with observations--cf. Tibaldi et al. 1990, Potter et al. 1993, and Sperber 1993.)

In DJF the largest model precipitation discrepancies also occur in the tropics (not shown). Here difference maps such as those of Fig. 1 suggest that there is less reason to recommend the T21 simulation of this season over those at T42-T106, since tropical discrepancies of similar magnitudes occur at all resolutions. Other global precipitation statistics suggest a more complex assessment of the different simulations. In DJF the histograms of pointwise departures of precipitation from the Legates-Willmott observations (Fig. 2) are negatively skewed at all resolutions, implying a general underprediction of precipitation that is especially prevalent over the oceans and in the Southern Hemisphere. This negative systematic bias is much less extreme at T21 (Fig. 2a), due primarily to the simulation of more precipitation in polar latitudes and over parts of Asia and North America than at T42-T106. (Comparable histograms for JJA do not display such biases.) On the other hand, the histograms at T42-T106 are much more sharply peaked around zero than at T21, indicating close agreement between simulated and observed precipitation at many more points in the higher-resolution simulations of DJF climate.

Convective vs. gridscale precipitation

In Fig. 3 global area-weighted averages of model precipitation and of its convective and gridscale components are shown as a function of resolution for both JJA and DJF. At all resolutions the simulated global-average precipitation is less than the value determined from the Legates-Willmott data, with that at T106 in best agreement with these observations. Agreement is also better at all resolutions in JJA (Fig. 3a)

than in DJF (Fig. 3b).

In both JJA and DJF the simulated global-average precipitation increases monotonically with resolution, but this similarity masks some marked differences in the resolution-dependence of the convective and gridscale components of precipitation. In both seasons gridscale precipitation decreases as the resolution increases beyond T21.

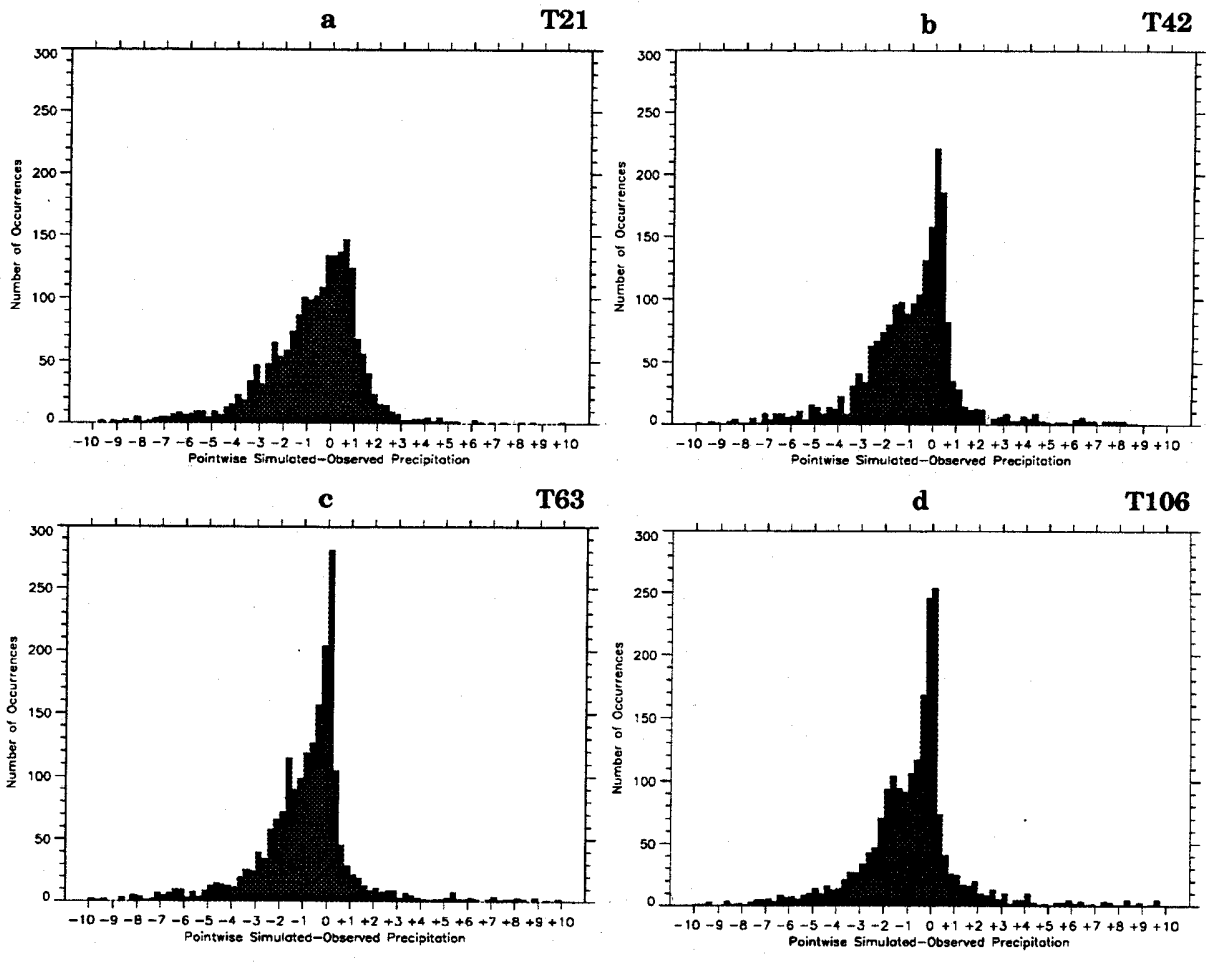

Fig 2. Histograms of pointwise departures of simulated precipitation (in mm day^{-1}) from the observations of Legates and Willmott (1990) for DJF simulations at resolutions T21 (a), T42 (b), T63 (c) and T106 (d), where b-d are interpolated to a T21 grid. (Note, these are *not* area-weighted departures.)

These decreases are offset by increases in convective precipitation that, in the global average, are monotonic with resolution, but that display different regional/seasonal

asymmetries. For example, in JJA convective precipitation decreases with resolution in the northern tropics (especially in the Asian monsoon region), but increases with resolution in the southern tropics due mainly to the presence of the spurious double ITCZ at T42-T106 (Figs. 1c-e).

In DJF, however, the zonal-mean convective precipitation in the equatorial southern tropics (the location of the upward branch of the seasonal Hadley cell) decreases as resolution increases beyond T21. Extratropical convective precipitation increases with resolution only in the winter hemisphere, but at all resolutions it is 20-30% greater in JJA than in DJF. Apparently this is because the simulated southern hemisphere winter storms are more convectively active than their northern hemisphere counterparts.

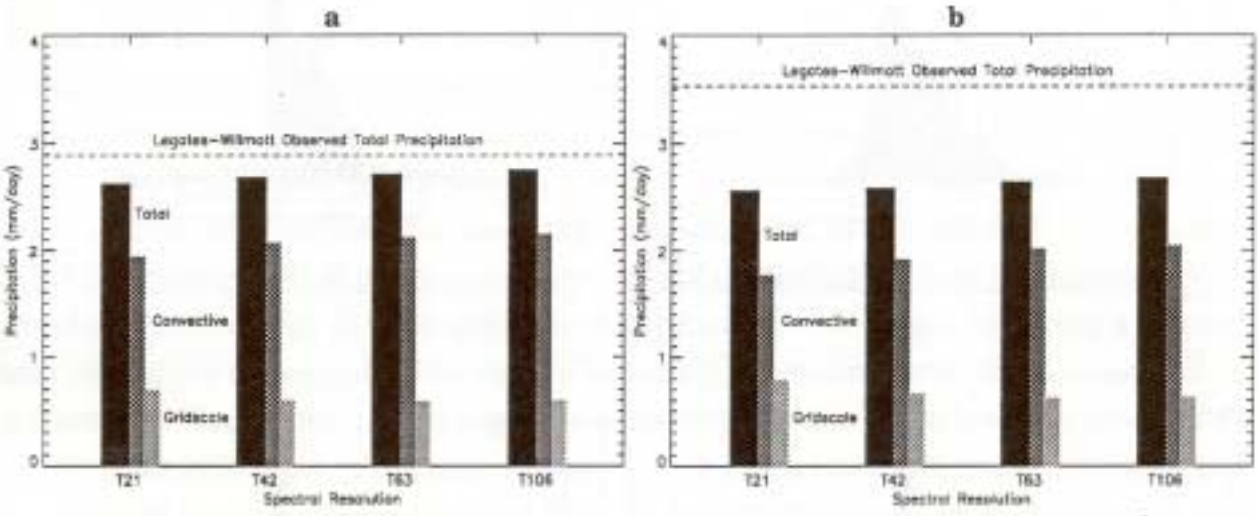

Fig. 3. Global area-weighted total precipitation and its convective and gridscale components (in mm day^{-1}) as a function of model resolution for JJA (a) and DJF (b). Global-averages of the Legates-Willmott (1990) observations of total precipitation also are shown for comparison.

The ratio of convective to total precipitation at T21 is mapped for JJA in Fig. 4a, and differences that appear with increasing resolution are shown in Figs. 4b-d. Nearly all (90-100%) of the model's tropical precipitation is due to convection (Fig. 4a), while in midlatitudes there is a variable mixture of convective and large-scale precipitation. In both hemispheres very little (< 10%) convective precipitation falls poleward of about 70 degrees, but in the northern hemisphere this precipitation type extends farther north over the (summer) continents than over the oceans, where convection is

damped by cold ocean currents and subsiding anticyclonic air to the west of the land masses.

In the model tropics there is little resolution-dependence in the ratio of convective to total precipitation (Figs. 4b-d), but in midlatitudes a decrease in convective precipitation just to the west of the continental boundaries accompanies an increase farther west. This pattern indicates that the gradient between a warm and cold surface and between rising and subsiding air at the continent-ocean boundaries is more sharply defined at the higher resolutions. Other extratropical changes with increasing resolution include more poleward penetration of convection over the northern continents and in the storm tracks of the southern (winter) hemisphere that result from decreases in gridscale precipitation and increases in convective precipitation (Fig. 3).

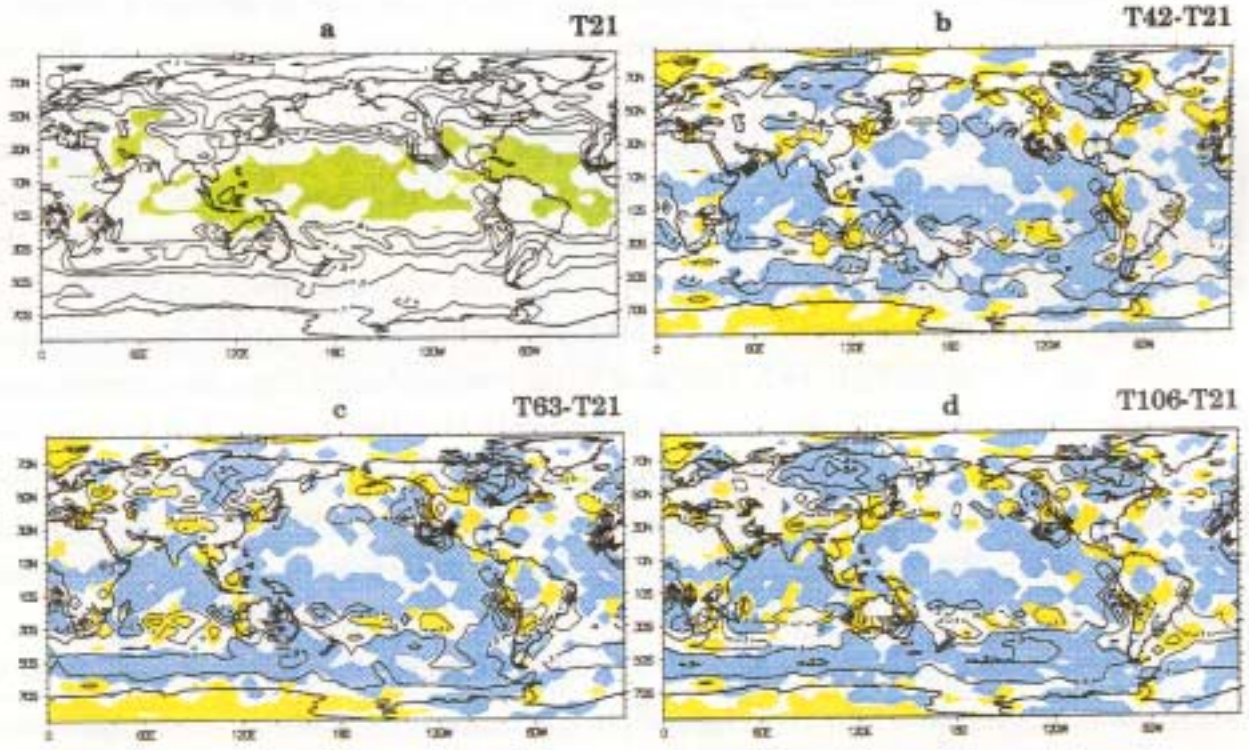

Fig. 4. JJA ratio of convective to total precipitation simulated at T21 resolution (a, with contours starting at 0.1 and spaced at intervals of 0.2, and with 1.0 values shaded green), and departures from the T21 values at resolutions T42 (b), T63 (c), and T106 (d). Lower ratios than at T21 with absolute values that are at least twice the interannual variability of the T42 simulation (not shown) are shaded yellow , while corresponding higher ratios are shaded blue. Difference contours start at ± 0.1 and are spaced at intervals of ± 0.2.

The spatial pattern of the DJF ratio of convective to total precipitation (not shown) is similar to that in JJA (Fig. 4a), except that the band of maximum values (ratio ≈ 1) is shifted southward, and the continental convective precipitation moves from the northern to the southern (summer) land masses. This ratio is also larger than that in JJA along the east coasts of the northern continents, where winter storm activity is most intense. As in JJA, the ratio of convective to total precipitation in DJF increases with resolution in the extratropics.

b. Atmospheric moisture

Precipitable water

The column-integrated atmospheric water vapor (i.e., the precipitable water) is a telling indicator of resolution-dependent variations in the moist processes. The observed field of this variable determined from 1987-89 National Meteorological Center (NMC) analyses (cf. Roads et al. 1992) is shown for DJF in Fig. 5a. It can be seen that precipitable water rapidly decreases poleward of about 30 degrees latitude, but there also are large zonal variations that reflect continent-ocean moisture contrasts and the sensitivity of surface evaporation to changes in ocean temperature.

Differences between simulations of DJF precipitable water and the observations of Fig. 5a are shown for T21, T42, T63, and T106 resolutions in Figs. 5b-e, respectively. It is obvious that the T21 simulation is too dry in the deep tropics, but further resolution increases only intensify this deficiency and extend the dryness farther poleward as well. A similar resolution-dependence is seen in the simulated precipitable water field for JJA (not shown), except that the extratropical drying is somewhat less severe.

Over the oceans a further check on the simulation of atmospheric moisture is to relate the precipitable water w (in kg m^{-2}) to the underlying sea surface temperature T_s (in deg K), as given by the relationship

$$w = 16.33\, e^{0.0686\,(T_s - 288)}$$

that was empirically determined by Stephens (1990) from analysis of 1979-82 Scanning Multiple Microwave Radiometer (SMMR) data. This comparison, shown for the model precipitable water in December, January and February in Fig. 6, confirms that

at all resolutions the ECMWF (cycle 33) model is too dry over the warmest ocean areas, but that overall the T21 simulation is most realistic: of a total of 3870 model data points on the common T21 grid, 1314 lie below the observed best-fit curve at T21; for the interpolated T42 to T106 fields the respective numbers are 1905, 1848, and 1821.

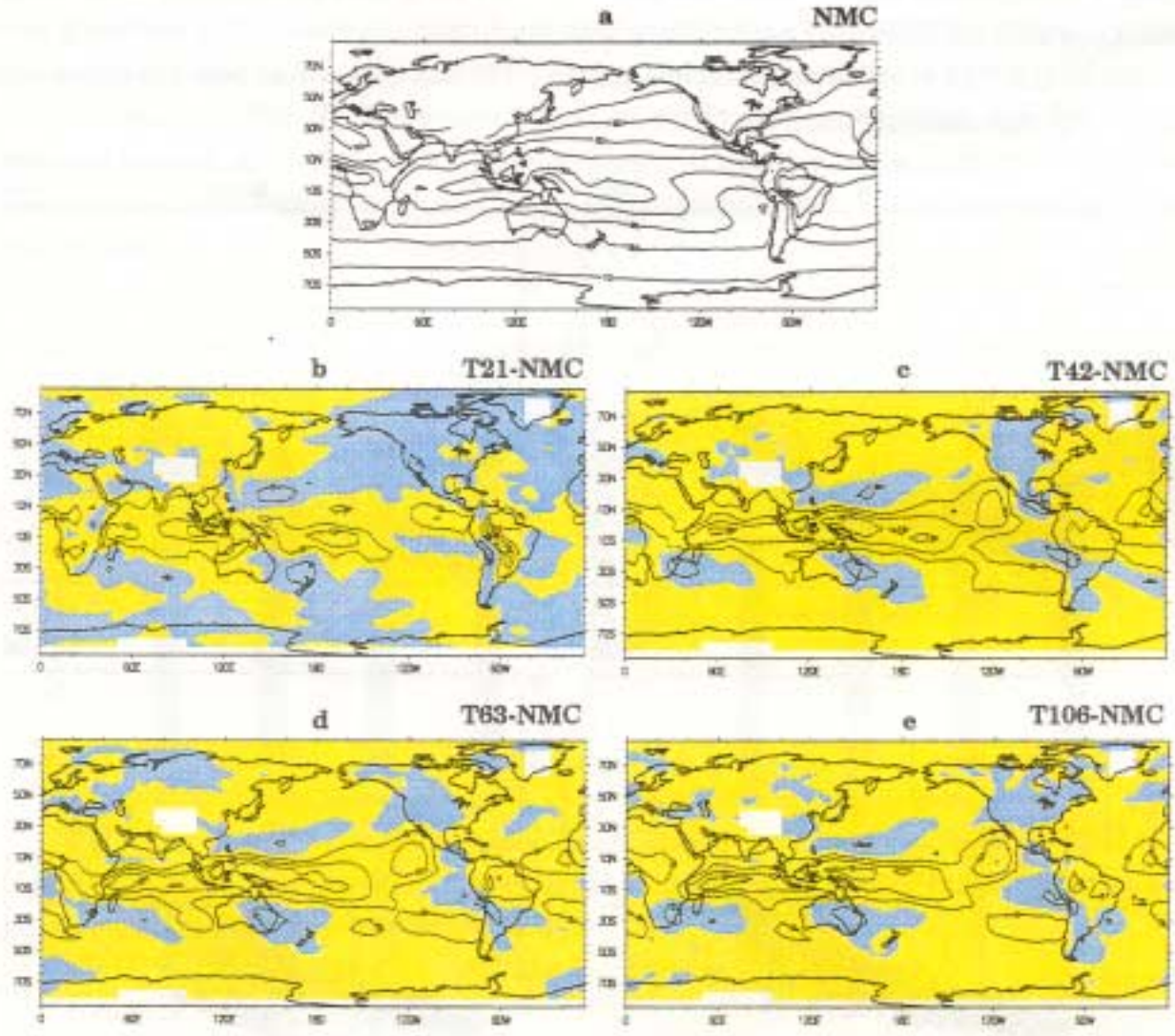

Fig. 5. DJF precipitable water from 1987-89 NMC analyses (a, with contours spaced at 10 kg m^{-2} intervals), and departures from the NMC values for simulations with resolutions of T21 (b), T42 (c), T63 (d), and T106 (e). Areas with less precipitable water than observed are shaded yellow, while areas with more precipitable water are shaded blue. Difference contours are spaced at ±5 kg m^{-2} intervals. Areas with unreliable or missing observational data appear in white.

In Fig. 7 global-average values of precipitable water at different resolutions are compared with those for the NMC observations in JJA and DJF. In agreement with Figs. 5 and 6, the global precipitable water in both seasons decreases as resolution increases beyond T21. However, the decrease is not monotonic with resolution: after a rather abrupt drop in the transition from T21 to T42, global precipitable water edges back towards its T21 value with subsequent resolution increases. This tendency to recover to the T21 level at resolutions T63 and T106 is somewhat less pronounced in DJF (Fig. 7b) than in JJA (Fig. 7a).

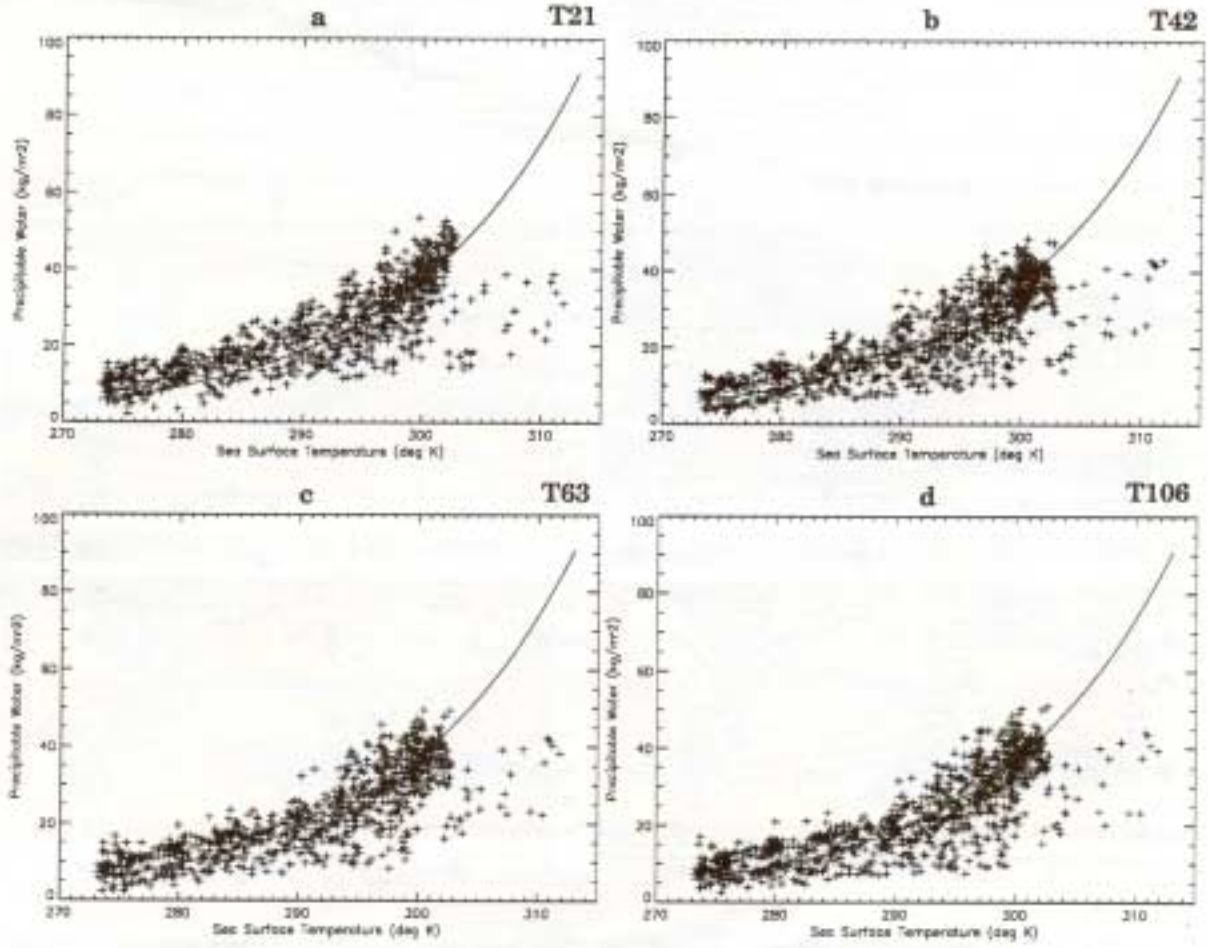

Fig. 6. Scatter plots of precipitable water (in kg m^{-2}) over the oceans in December, January, and February as a function of underlying sea surface temperature (in deg K) at resolutions T21 (a), T42 (b), T63 (c), and T106 (d), with values for b-d interpolated to a T21 grid. The best-fit empirical relationship (solid curve) obtained by Stephens (1990) from 1979-82 SMMR passive microwave radiometry data is also shown for comparison.

Comparison of Figs. 3 and 7 reveals that in both DJF and JJA the global precipitation increases with resolution in spite of overall decreases in precipitable water. This is due to the steadily increasing global convective precipitation with resolution (Fig. 3), an indication that the model's subgridscale convective processes are decoupled to some extent from the large-scale atmospheric moisture field. However, the global gridscale precipitation (Fig. 3) is clearly affected by the atmospheric drying, although it does not fall off proportionally to the variation of global precipitable water with resolution (Fig. 7). Apparently because gridscale precipitation is a function of vertical motion as well as atmospheric moisture, there is not a high correlation between the variations of precipitation and precipitable water with increasing model resolution.

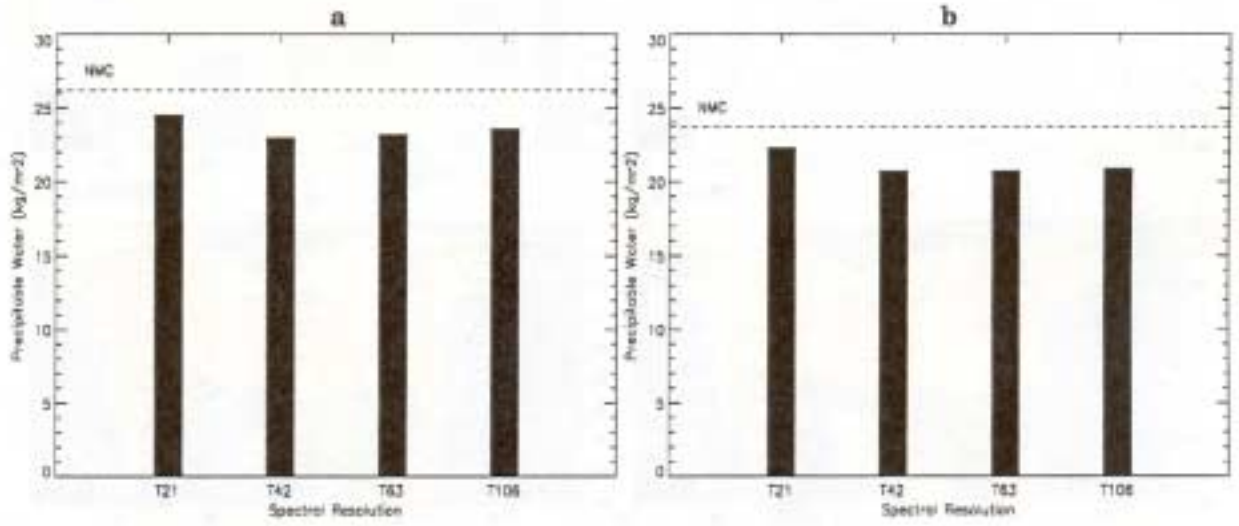

Fig. 7. Global area-weighted averages of simulated precipitable water (in kg m^{-2}) in JJA (a) and in DJF (b) as a function of resolution. Area-weighted values derived from NMC analyses averaged over the period 1987-89 also are shown for comparison.

Relative humidity

Atmospheric relative humidity is also of pivotal importance in the ECMWF model, since the amount of gridscale nonconvective cloud is diagnostically determined from this moisture variable. The zonal-mean profile of DJF relative humidity is shown at T21 in Fig. 8a, and departures from this at resolutions T42, T63, and T106 in Figs. 8b-d, respectively. As the resolution increases beyond T21, there are substantial changes in the relative humidity profile: equatorial humidity at upper levels

increases as tropopause temperature decreases, but tropical/subtropical air elsewhere becomes progressively drier. In high latitudes, however, relative humidity increases with resolution in spite of decreases in absolute humidity (Figs. 5c-e). This occurs in association with an intensifying cold bias in atmospheric temperatures (Boyle 1993), a common but poorly understood feature of many GCM climate simulations (Boer et al. 1991). Analogous but somewhat less pronounced changes in relative humidity accompany the resolution increases in JJA (not shown).

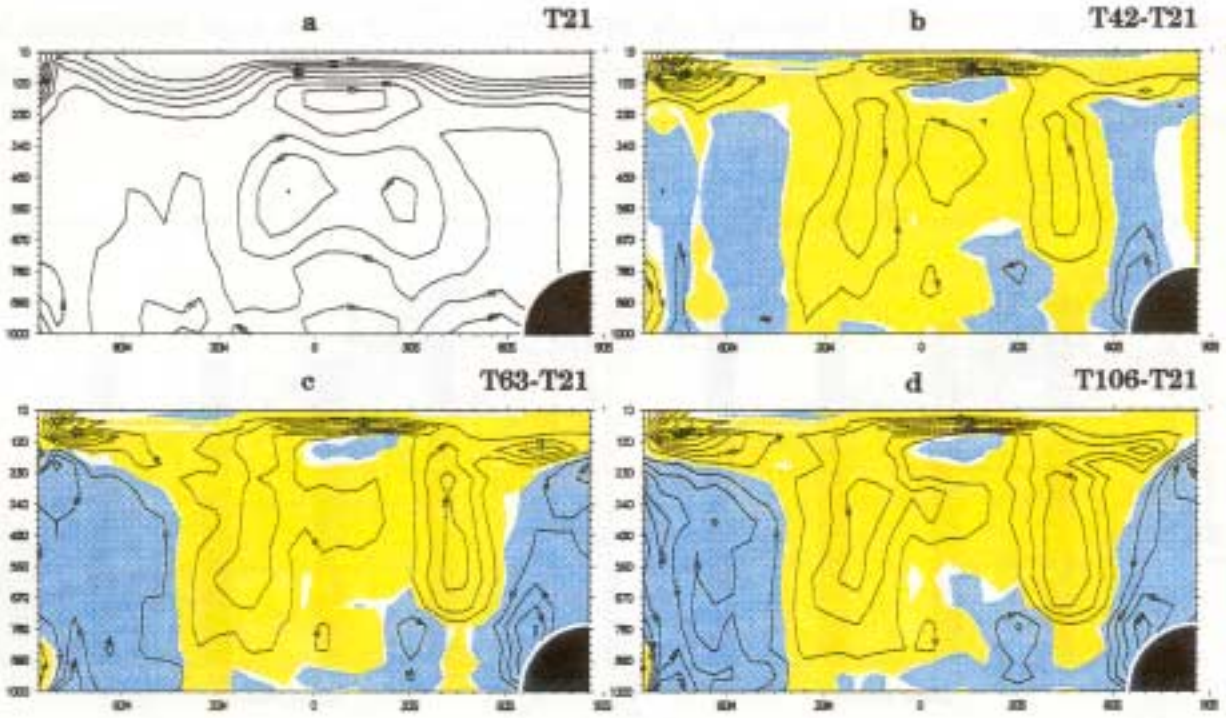

Fig. 8. Zonal-mean profile of DJF atmospheric relative humidity (in %) simulated at T21 resolution (a, with contours spaced at 10% intervals), and departures from the T21 values at resolutions T42 (b), T63 (c), and T106 (d). Areas with lower humidity than at T21 with absolute values that are at least twice the interannual variability of the T42 simulation (not shown) are shaded yellow, while corresponding areas of higher humidity are shaded blue. Difference contours are spaced at ± 5% intervals.

Moisture convergence

Heavy precipitation usually accompanies strong convergence of atmospheric moisture. In the ECMWF (cycle 33) model the major centers of moisture convergence in JJA are located in the Asian monsoon region and near Central America. The convergence field of precipitable water is shown for the first of these centers at T21 in

Fig. 9a and at T42-T106 (uninterpolated) in Figs. 9b-d respectively. At T21 there is moisture convergence over the whole region (Fig. 9a), while at the higher resolutions the maximum convergence is much stronger, but is confined mostly to the Tibetan plateau (Figs. 9b-d). As in the results reported by Tibaldi et al. (1990) and Sperber (1993), the T21 simulation does not resolve the effects of the small-scale orography such as the local divergence of moisture leeward of the Ghats Mountains of southwest India (Fig. 9a) that are visible at resolutions T42-T106 (Figs. 9b-d). Nevertheless, the T21 model produces the most realistic simulation of large-scale monsoonal precipitation (Fig. 1b).

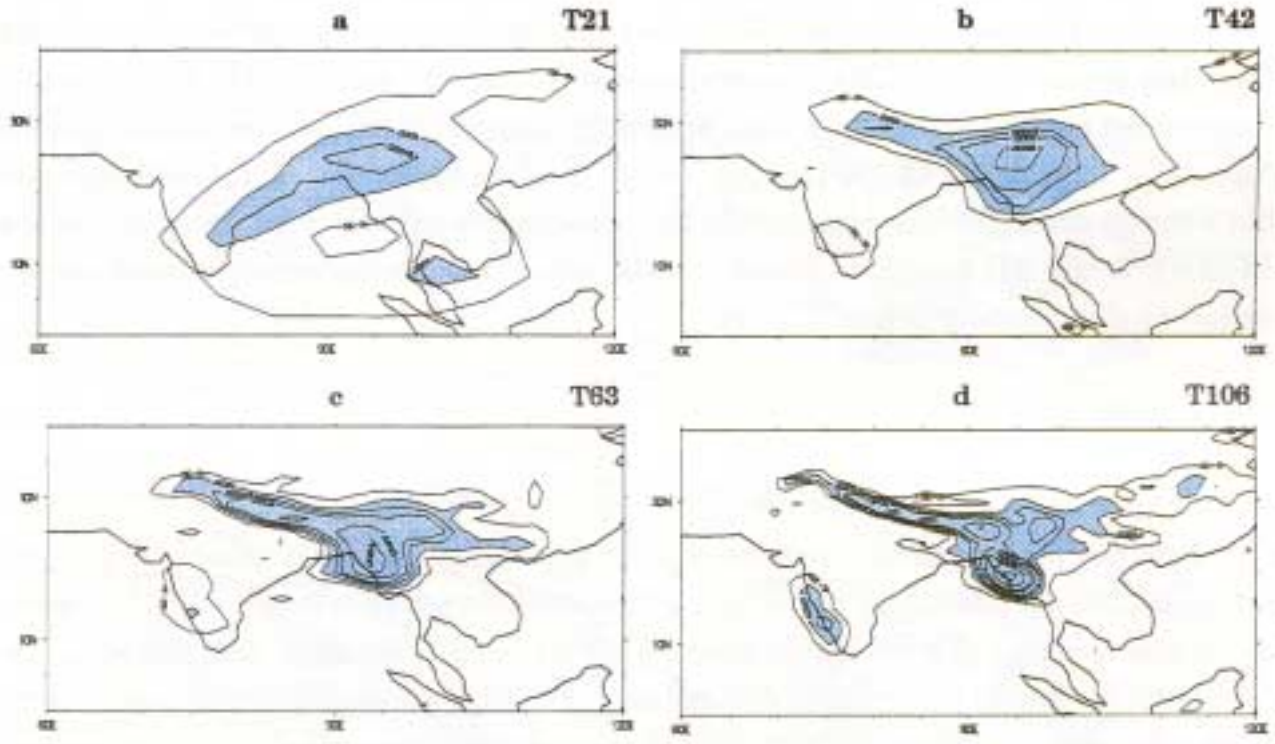

FIG. 9. Convergence of precipitable water simulated during JJA in the Asian monsoon region at T21 resolution (a), and (uninterpolated) at T42 (b), T63 (c), and T106 (d). Contours are at 0.5,1,1.5,2,3,4,6, and 8×10^{-4} kg m^{-3}, with values greater than 1×10^{-4} kg m^{-3} shaded blue.

The increasing noisiness of the moisture convergence field at resolutions finer than T21 that was noted by Tibaldi et al. in the ECMWF (cycle 28) model is also apparent in Figs. 9b-d. This similarity occurs in spite of a major change in the parameterization of deep convection from the modified Kuo scheme in ECMWF (cycle 28) to

the Tiedtke (1989) mass-flux scheme in ECMWF (cycle 33). Moreover, Battisti et al. (1991) found that the Kuo convective scheme tends to produce a double ITCZ structure, which is a dominant feature of the ECMWF (cycle 33) JJA tropical climate at resolutions T42-T106. Thus, although the Tiedtke and Kuo convective parameterizations are different in many respects, they seem to experience similar difficulties in capturing certain features of the observed tropical climate at resolutions finer than T21. These shortcomings may originate from the provision of moisture-convergence closure that is common to both convective schemes.

In the ECMWF (cycle 33) model another possible factor contributing to the deficient JJA monsoon precipitation at T42-T106 is that the marine low-level winds are too weak in this region (Boyle 1993), thus depressing the evaporation of moisture from the ocean surface. This evaporation deficit may be attributable to increasing drag on the surface winds from local orography that is better resolved at resolutions finer than T21 (Rao et al. 1991). Gleckler and Taylor (1993), however, found that global-average ocean surface evaporation increased monotonically with resolution in the ECMWF (cycle 33) model, as should be the case for a corresponding monotonic increase in global precipitation (Fig. 3).

c. Clouds

Convective cloud

Because precipitation is not universally associated with convection, cloud properties can supply additional important information on convective activity. For example, the percentage of time that convective clouds occur (hereafter, designated as the "convective frequency") in the JJA simulation at T21 is shown in Fig. 10a. Here convective frequency is highest ($\geq 80\%$) in the Asian monsoon region and in the central Pacific between latitudes 10 S to 25 N. The convective frequency at T21 is also high ($\geq 60\%$) in most other tropical ocean areas and in the latitudes of the southern (winter) storm tracks; it also seems unrealistically high in some parts of Antarctica ($\geq 40\%$). At T21 the convective frequency is relatively low ($\leq 50\%$) in the dry subsiding air over the southern subtropical oceans and, more surprisingly, over the northern continents where the ratio of convective to total precipitation is substantial (Fig. 4a). Apparently, when model convection does occur over the summer continents relatively

intense precipitation results.

Differences between the JJA convective frequency at T42, T63, and T106 resolutions and that at T21 are shown in Figs. 10b-d, respectively. The largest negative departures occur in the Asian monsoon region, consistent with the scant precipitation simulated here at the higher resolutions (Figs. 1c-e); the decreased convective activity over Antarctica at T42-T106 (Figs. 10b-d) is probably more realistic, however. At the higher resolutions substantially greater convection occurs near Central America and Australia, in the central North Pacific, poleward of 50 S, and in some Arctic regions. The intensification of the latter two centers at T63 and T106 implies that JJA convective frequency at high latitudes is enhanced by increasing resolution.

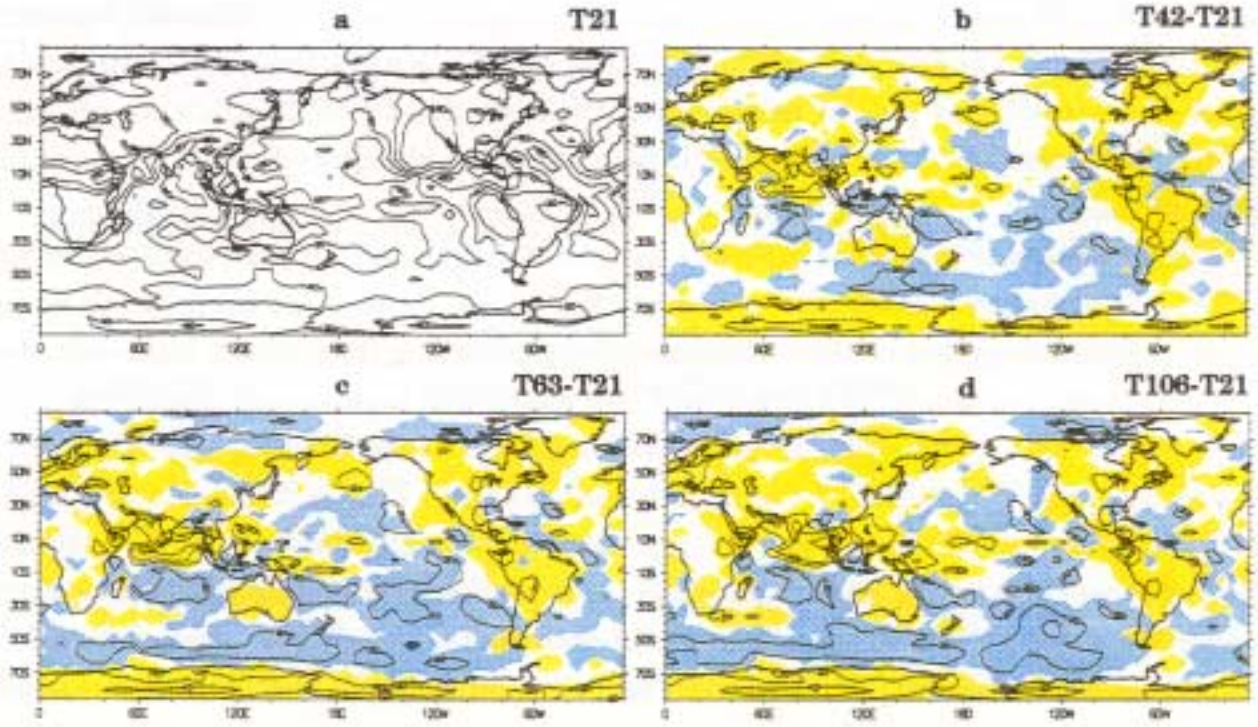

Fig. 10. The frequency of convective clouds (in %) simulated during JJA at T21 resolution (a, with contours at 20% intervals), and departures from these T21 values at resolutions of T42 (b), T63 (c), and T106 (d). Convective frequencies lower than at T21 with absolute values that are at least twice the interannual variability of the T42 simulation (not shown) are shaded yellow, while corresponding higher convective frequencies are shaded blue. Difference contours are spaced at intervals of ±20%.

In DJF at T21 resolution (not shown) a continuous band of high convective activity stretches from the Indian Ocean eastward across the Pacific to the Atlantic. Other

centers of high convective frequency lie to the west of South America and along the northern (winter) storm tracks. The only substantial continental convective centers in DJF are located over the Amazon basin and southern Africa. As in JJA, with increasing resolution convective clouds form more frequently at high latitudes.

Convective cloud-base and cloud-top pressures were also archived for the different resolutions. Convective cloud base pressure is relatively insensitive to changes in resolution, while cloud-top pressure--a measure of the intensity of penetrative convection in the model--is more responsive to increasing resolution.

Maps of the pressure levels of all (convective and nonconvective) clouds observed with tops above 500 hPa from the 1983-88 International Satellite Cloud Climatology Project (ISCCP) data are shown for JJA in Fig. 11a. In this season clouds likely to be associated with convection are observed over North, Central and South America, southern Asia, the Indian and equatorial West Pacific Oceans, and equatorial/southern Africa. (It is likely that at least part of the high cloud over the Tibetan plateau, the Rocky Mountains, and Antarctica is nonconvective cloud produced by orographic uplift.)

The pressure levels of the model's convective cloud tops that penetrate above 500 hPa in JJA are shown at all resolutions in Figs. 11b-e. From these maps it can be inferred that the increases in convective frequency occurring in southern high latitudes at resolutions finer than T21 (Figs. 10b-d) are associated mainly with shallow or mid-level convection (i.e., convective tops below 500 hPa). The spatial pattern of convective cloud above 500 hPa in the T21 simulation of JJA (Fig. 11b) is in qualitative agreement with the ISCCP data (Fig. 11a), but there is more cloud above 500 hPa than is observed over northern Africa, the Caribbean and the interior of Asia. Much of this convective cloud also penetrates to levels higher than observed (i.e., above 400 hPa).

These discrepancies persist in the T42-T106 simulations (Figs. 11b-e), but in addition there is too much high convective cloud over South America and north of Australia, where the southern branch of the spurious double ITCZ is situated. At T42-T106 cloud-top heights are lower than observed over at least part of the Asian monsoon region and the equatorial West Pacific, consistent with the undersimulation of convection (Figs. 10b-d) and precipitation (Figs. 1c-e) in these regions. At T42 the absence of penetrative cloud in the equatorial West Pacific is especially noticeable (Fig. 11c), and there also is too much convective cloud over northern Africa. These and other discrepancies ameliorate somewhat at T63 and T106 resolutions (Figs. 11d-e).

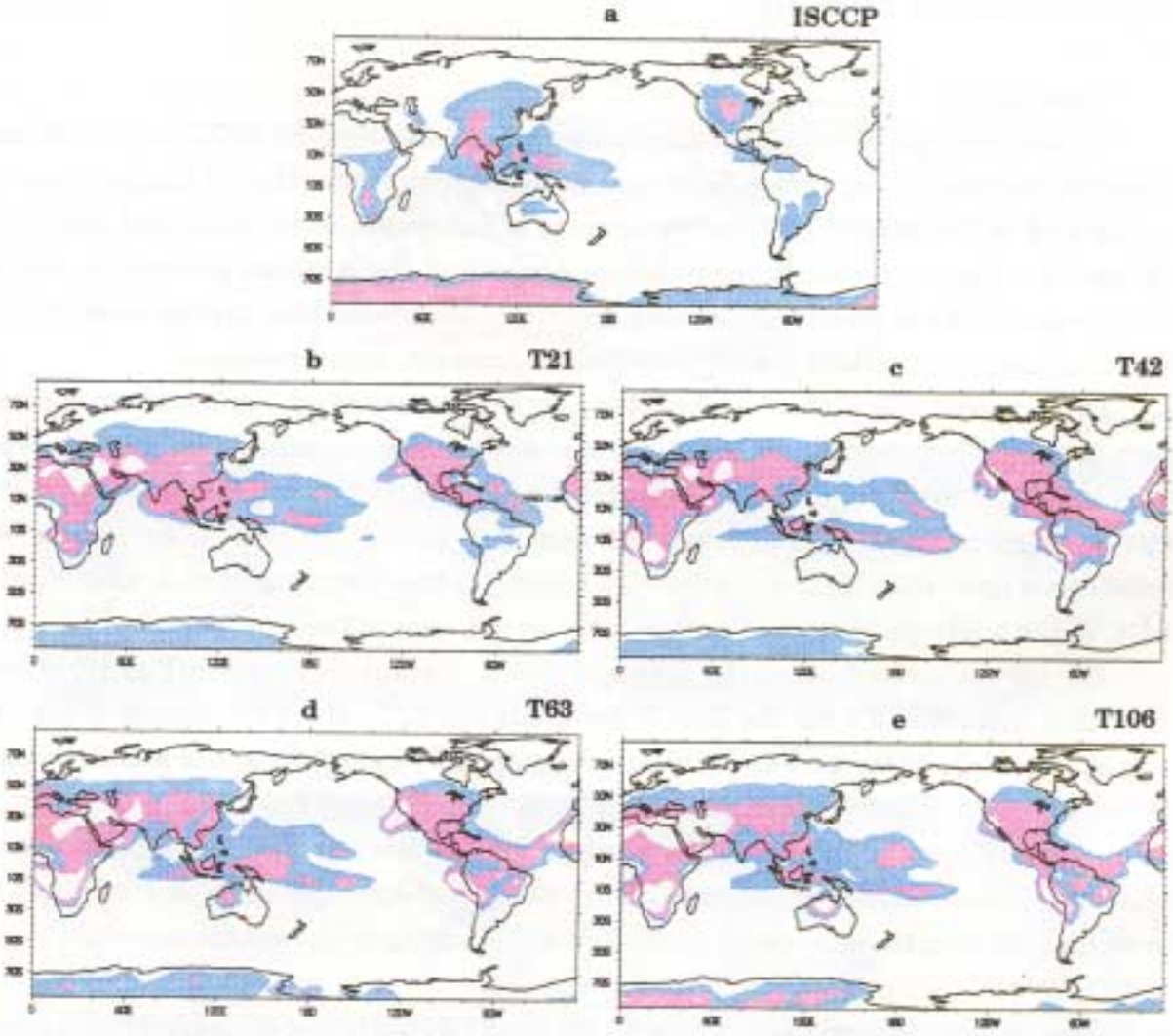

Fig. 11. 1983-88 ISCCP satellite observations of pressures of all cloud tops that are at or above 500 hPa in JJA (a), and convective cloud-top pressures at or above 500 hPa for JJA simulations at T21 (b), T42 (c), T63 (d), and T106 (e). Cloud between 500 and 400 hPa is shaded blue and cloud above 400 hPa is shaded violet.

In DJF (not shown) the highest clouds are associated with the major convective centers in Indonesia, Amazonia and southern Africa, with the center of penetrative convection above the equatorial West Pacific warm pool being especially prominent.

Again the T21 simulation displays the best overall agreement with the ISCCP observations of cloud-top pressures.

Total cloud

Top-of-atmosphere total cloud cover estimated from 1983-88 ISCCP observations is shown for DJF in Fig. 12a. Clouds are most extensive over the midlatitude storm tracks and in the tropical convective centers of Indonesia, Amazonia, and southern Africa. Cloud cover is scant over Saharan Africa and the Arabian peninsula, and in the equatorial East Pacific. Relatively clear-sky conditions also prevail over China and the Asian subcontinent, southwest North America, and Greenland.

In the model (Figs. 12b-e) global cloud cover is too scant over much of the oceans, but appears to be generally too extensive over the continents, especially in middle and high latitudes. While similar model deficiencies are apparent at all resolutions, the T21 simulation (Fig. 12b) is in best agreement with the ISCCP cloud observations. At resolutions finer than T21, cloud cover decreases in the deep tropics and, most markedly, in the subtropical marine anticyclones to the west of the continents.

For all model resolutions the seasonal global-average cloud cover (Fig. 13) is less than that determined from the ISCCP data, but the T21 values are closest to the observations while those at T42-T106 are substantially below observations. Although global cloud cover decreases rather abruptly in the transition from T21 to T42, it edges upward slightly at T63 resolution and somewhat more at T106. It should be emphasized, however, that at all resolutions the global-average value is the result of oversimulated continental cloud partially compensating undersimulated ocean cloud (Figs. 12b-e).

From comparison of Figs. 13a and 13b, the ECMWF (cycle 33) global cloud cover is somewhat less sensitive to resolution increases in JJA than in DJF, in that the T21 to T42 decrease is more abrupt in the latter season. This seasonal dependence is consistent with that of the global precipitable water (Fig. 5). Previous studies of the impact of resolution on GCM moist processes did not investigate a possible seasonal modulation in cloud cover, since only annual-mean (Rind 1988), January-mean (Kiehl and Williamson 1991), or July-mean (Morcrette 1991) model climates were analyzed. The July global cloud cover reported by Morcrette for the ECMWF (cycle 36) model showed even less quantitative sensitivity to resolution increases than that of Fig. 13a, probably because of new parameterizations of surface evaporation (Miller et al. 1992)

and nonprecipitating convective clouds that were introduced in the ECMWF (cycle 36) model.

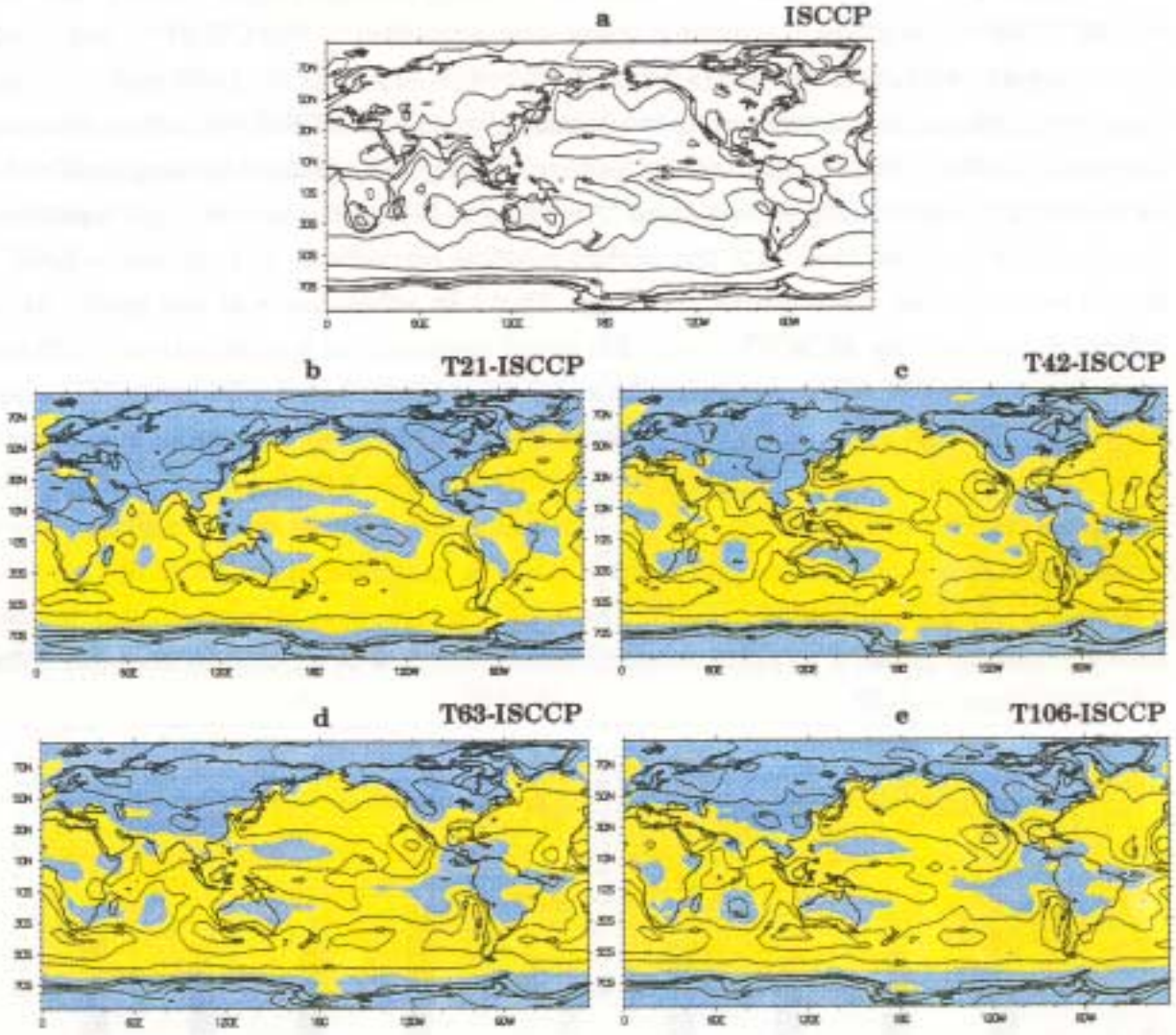

Fig. 12. 1983-88 ISCCP satellite observation of DJF total cloud cover (a, with contours at 20% intervals), and departures from these observation for simulations at resolutions of T21 (b), T42 (c), T63 (d), and T106 (e). Areas with more cloud cover than observed are shaded blue, while areas with less cloud cover are shaded yellow. Difference contours are spaced at ± 20% intervals.

The zonal-mean profile of total cloud amount is shown in Fig. 14 for the ECMWF (cycle 33) model. (Because neither convective cloud amounts nor the three-hourly

accumulations of precipitation from which these amounts could be derived were saved in the simulation archives, the convective portion of these cloud profiles is approximated from six-hourly snapshots of convective precipitation.) In the Hadley regime of the ECMWF (cycle 33) model a mechanism similar to that in the CCM1 appears to be operating as resolution increases beyond T21. For example, in DJF mid-level and high-level tropical and subtropical clouds mostly decrease as the resolution increases beyond T21 (Figs. 14b-d) because of a general drying of the model atmosphere at low latitudes (Figs. 5c-e). (An exception to this pattern is the increase in high equatorial cloud, which is associated with the higher relative humidities at tropopause level in the finer-resolution simulations--see Figs. 8b-d.) In other parts of the model atmosphere, however, the ECMWF (cycle 33) cloud responds in a qualitatively different way than the CCM1 to the resolution increase. For example, in high latitudes of both hemispheres cloud amount increases at most levels; low-level cloud also increases in midlatitudes, and extends progressively farther into the subtropics as resolution increases from T42 to T106 (Figs. 14b-d). The net effect of these changes is that somewhat more top-of-atmosphere global cloud cover is produced in the ECMWF model at T63 and T106 than at T42 (Fig. 14b). The clouds in JJA (not shown) display a qualitatively similar pattern as resolution increases, but low-level clouds increase somewhat less than in DJF.

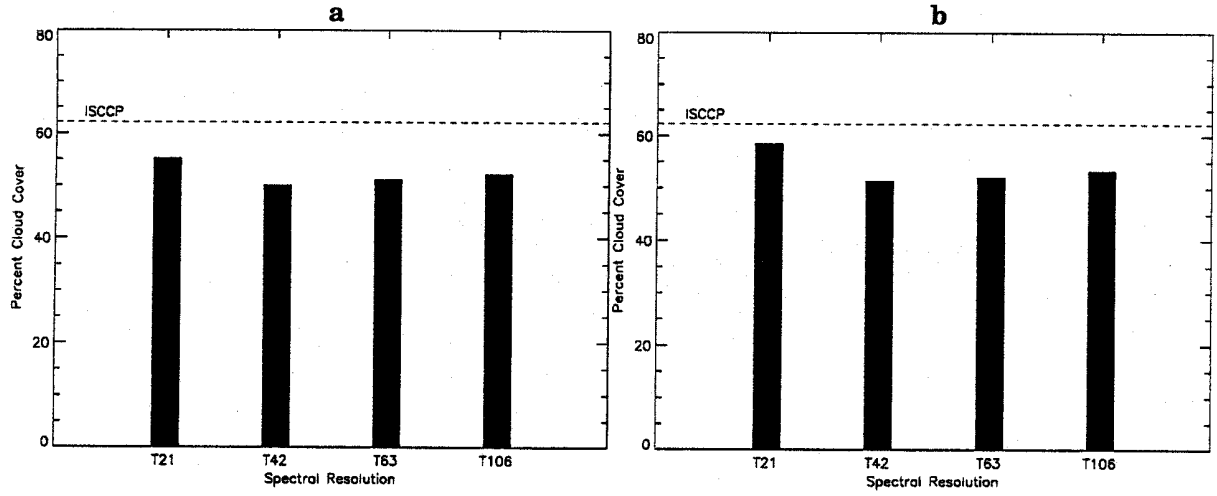

Fig. 13. Global area-weighted cloud cover (in percent) as a function of resolution for JJA (a) and for DJF (b). Global values derived from ISCCP satellite observations are shown for comparison.

Most of the resolution-dependent changes in DJF (and JJA) cloud profiles in the ECMWF (cycle 33) model (Figs. 14b-d) are similar to those seen in the relative humidity field (Figs. 8b-d), but there are a few exceptions. These include the decrease in mid-level cloud in high northern latitudes that occurs in the presence of increased humidity, and the enhancement of low-level subtropical cloud in the presence of decreased humidity. The likely causes of these anomalies can be inferred by separating the cloud that forms in regions of upward motion from that which forms in regions of downward motion--a diagnostic also utilized by Kiehl and Williamson (1991) for the CCM1 model.

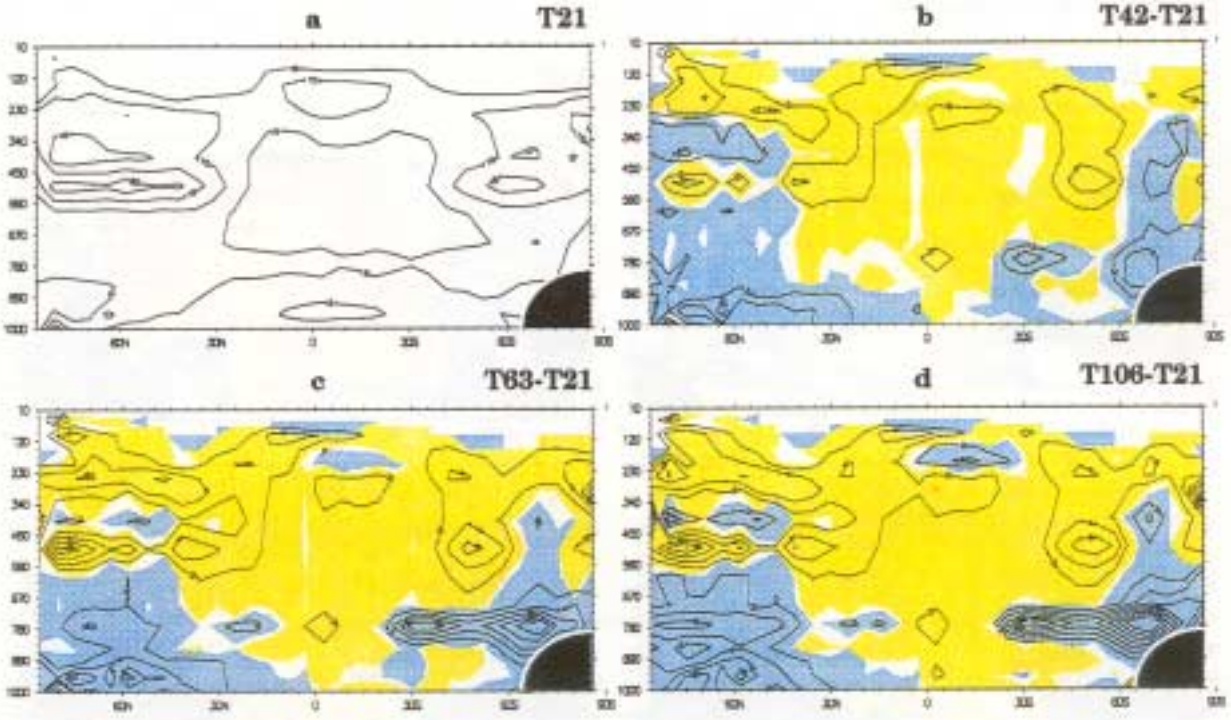

Fig. 14. Zonal profile of DJF cloud amounts for the T21 simulation (a,with contours spaced at 5% intervals), and departures from these T21 values at T42 (b), T63 (c), and T106 (d). Areas with less cloud than at T21 with absolute differences that are at least twice the interannual variability of the T42 simulation (not shown) are shaded yellow, while corresponding areas with more cloud are shaded blue. Difference contours are spaced at ±2 % intervals. The convective-cloud portions of these profiles are approximated from six-hourly snapshots, rather than 3-hourly accumulations, of convective rainfall.

The zonal-mean profiles of these "cloud-up" and "cloud-down" stratifications are shown in Figs. 15 and 16, respectively. Except near the pole, where upward vertical

motion at T42-T106 is less intense than at T21 (Figs. 15b-d), the decrease of mid-level cloud in northern high latitudes with resolution is mainly due to depressed cloud formation in regions of downward vertical motion (Figs. 16b-d). This may occur because of a reduction in gridscale cloud in response to downdrafts from convective systems (as required by the Slingo 1987 cloud-formation scheme) which intensify with resolution at these latitudes in DJF. In contrast, with increasing resolution low-level cloud that forms in regions of downward motion increases and spreads from higher latitudes toward the subtropics (Figs. 16b-d). Since this low-level cloud can form in subsiding air only when temperature inversions are present (Slingo 1987), the intensity and/or frequency of such inversions in the ECMWF (cycle 33) model apparently increases with resolution.

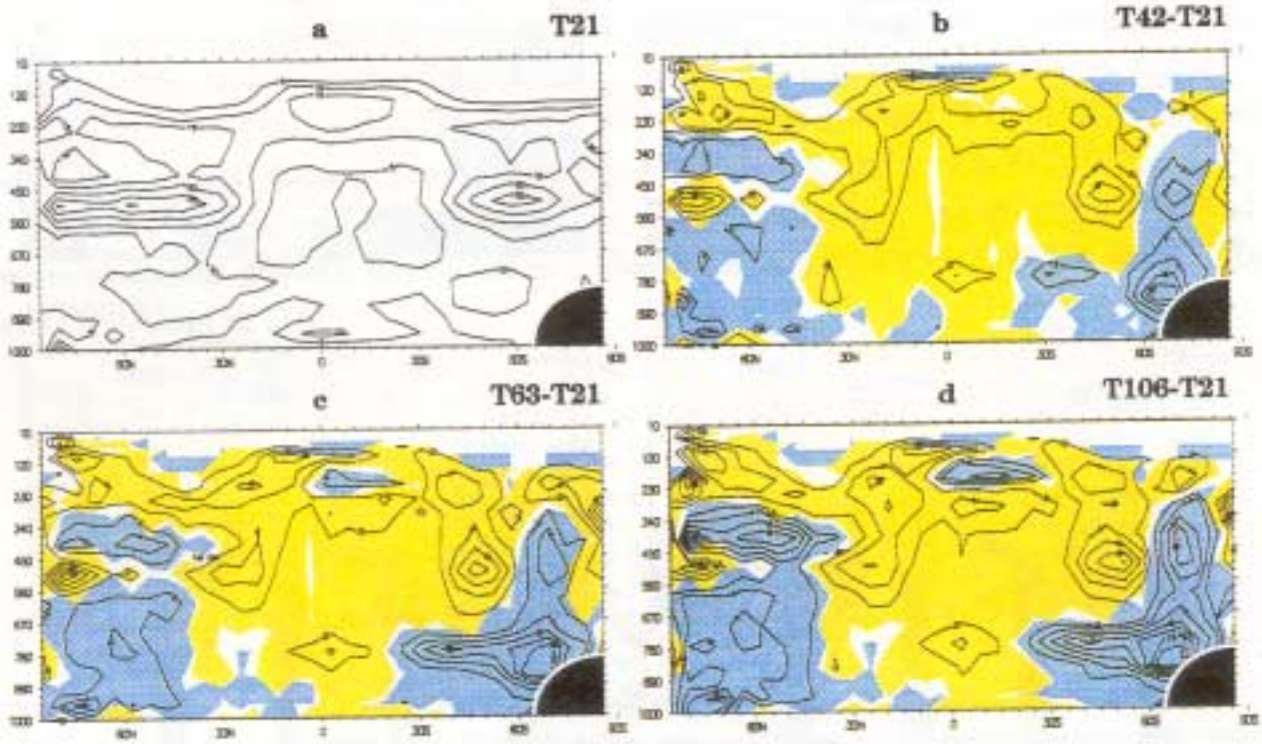

Fig. 15. As in Fig. 14, except for DJF total cloud in regions of upward vertical motion only. (In a, contours are spaced at 5 % intervals, and at ±2 % intervals in b-d.)

It is noteworthy that Kiehl and Williamson (1991) reported resolution-dependent changes in extratropical relative humidity (and in atmospheric cold bias) that were qualitatively similar to those seen in the ECMWF (cycle 33) model (Figs. 8b-d);

yet, in most latitudes, CCM1 cloud amount decreased with resolution. Perhaps this was because the threshold humidity for cloud formation in the CCM1 was set at 100% rather than the 80% value used in the ECMWF model, and therefore changes in CCM1 clouds with increasing resolution may have been related more to changes in vertical motion and/or in advection of moisture than to changes in local relative humidity. Moreover, the CCM1 cloud formation scheme did not include a mechanism for producing cloud in the presence of temperature inversions, so that the increase in subtropical low-level cloud with resolution observed in the ECMWF (cycle 33) model could not occur. (In fact, this type of cloud was depleted most when resolution increased in the CCM1.)

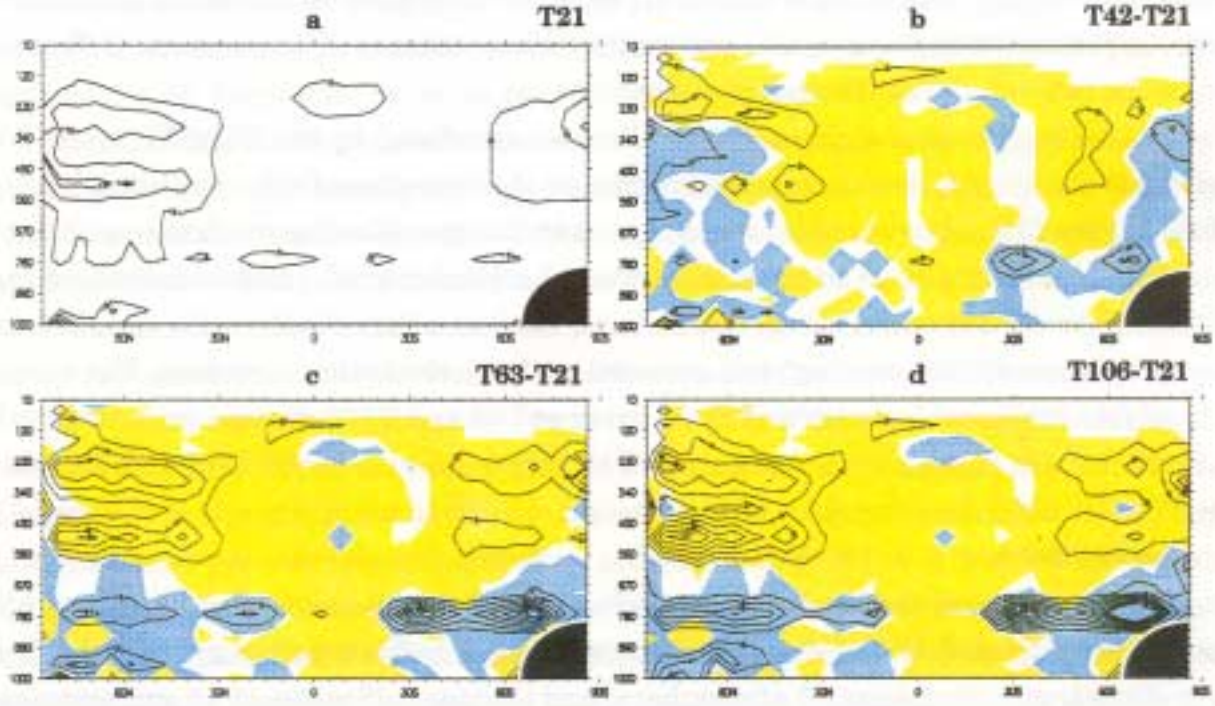

Fig. 16. As in Fig. 15, except for DJF cloud in regions of downward vertical motion. (In a, contours are spaced at 5 % intervals, and at ±2 % intervals in b-d.)

4. Summary and concluding remarks

We have seen there are a number of subtleties in the response of moist processes to increasing horizontal resolution in the ECMWF (cycle 33) model. As resolution increases the model atmosphere tends to dry out, but precipitation (and evaporation) steadily increase, subgridscale convective processes intensify, and cloud amounts increase in some regions. Many of the largest changes occur in the tropics, where deep convection plays a central role, but there are also marked changes in extratropical precipitation, relative humidity, and cloud amount that accompany the resolution increases. Some resolution-dependent changes are modulated by season as well; for example, precipitable water and cloud cover are somewhat more sensitive to resolution increases in DJF than in JJA. However, seasonal asymmetries in extratropical convective precipitation occur at all resolutions, mainly because of hemispheric differences in the intensity of convective processes.

A striking feature of the seasonal climates simulated by the ECMWF (cycle 33) model is the qualitative change that occurs in the transition from resolution T21 to T42, followed by only quantitative changes in the large-scale climatic features at finer resolutions; this result is in agreement with the Tibaldi et al. (1990) analysis of the ECMWF (cycle 28) model. It cannot be said, however, that the cycle 33 simulations are progressively "converging" to a common state as resolution increases. For example, global precipitable water and cloud cover at T63 and T106 diverge from their values at T42 and move back toward their T21 values (cf. also Boyle 1993 and Gleckler and Taylor 1993 for discussion of analogous behavior in other aspects of the model's seasonal climates).

Some of the resolution-dependent effects noted in this study also have been observed in other models. For example, the enhancement of convective activity, the drying of the tropical/subtropical atmosphere, and the intensification of an extratropical cold bias appear to be common model responses to resolution increases (Rind 1988, Kiehl and Williamson 1991, Morcrette 1991). In addition, these prior studies all have noted a tendency for model cloud cover to decrease with increasing resolution; however, the details of resolution-dependent changes in simulated clouds appear to be highly model-specific. In the GISS model, for example, mainly cirrus clouds were affected by resolution changes (Rind 1988), while in CCM1 low subtropical cloud was most sensitive. In the ECMWF (cycle 33) model a decrease in cloud cover brought about by

enhanced drying of the atmosphere in low latitudes as resolution increases is partially offset by increased high-latitude cloud cover that results from an intensified cold bias and associated changes in relative humidity. The amount of low-level midlatitude and subtropical cloud that forms in regions of downward motion also increases with resolution, in contrast to their behavior in the CCM1 model.

It is sobering that, in spite of common resolution-dependent mechanisms at work in several different GCMs, the simulated clouds show such diverse sensitivity to resolution changes. There is scant comfort to be derived, for example, from the fact that global cloud cover in the ECMWF model is considerably less sensitive to resolution changes than in the CCM1, since this is mainly the outcome of a model-specific response to a systematic error (i.e., an atmospheric cold bias). Progress in simulating clouds in climate models may have to await further development of prognostic cloud-formation schemes (e.g., Sundqvist 1978) that are more physically based than the semi-empirical diagnostic methods presently used in most GCMs.

Finally, this study demonstrates that an improved simulation of the moist processes does not result simply from increasing the horizontal resolution; in fact, the T21 simulation of *large-scale* tropical seasonal climate appears to be generally in best agreement with the available observations. It should not be concluded, however, that T21 resolution is sufficient for a faithful simulation of global climate. T21 integrations poorly represent the transient behavior of the atmosphere and exhibit more deficiencies in the extratropical dynamical fields than T42-T106 simulations (Tibaldi et al. 1990, Boyle 1993). There are indications as well that simulations at resolutions higher than T21 are necessary to capture seasonal climate and intraseasonal variability in regions that are strongly influenced by orography (Tibaldi et al. 1990, Potter et al. 1993). Certainly the keenly felt need for credible climate simulations on regional scales will continue to be a strong motivation for using the highest resolution that is computationally feasible. The point is not to "settle" for T21 resolution in climate applications, but to improve the performance of GCMs at resolutions that are high enough to meaningfully simulate the details of regional climates.

Although we cannot discount the possibility that the more realistic simulation of large-scale tropical climate at T21 is merely a result of a fortuitous compensation of errors, the higher quality of the T21 simulation may be related to a better matching of the scales implicit in the physical parameterizations with the model's explicit horizontal resolution. For example, when the convective parameterization is based on a

moisture-convergence closure assumption such as in the Tiedtke (1989) scheme, the seasonal-mean transfer of divergent kinetic energy from the convective scale to the large scale in the tropics may be better simulated at T21 than at finer resolutions. These results seem surprising in view of the use of T106 as the standard resolution for the operational ECMWF (cycle 33) model, but reflect the different criteria for judging the performance of a model designed primarily for accurate extratropical weather forecasting at time scales of 1 to 15 days rather than the simulation of tropical seasonal climate.

It is possible that the ECMWF (cycle 33) model would perform better for climate simulation at higher resolutions if its physical parameterizations were suitably "tuned". For example, there is preliminary evidence from the ECMWF (cycle 36) model that minor changes in the parameterizations of surface evaporation and cloud formation produce substantial improvements in the simulated climate at T106 resolution (Miller et al. 1992). There is, however, some contrary evidence on the benefits of tuning the convective parameterization, since the ECMWF (cycle 36) model seems fairly insensitive to changes in convective schemes, at least with respect to the simulation of clouds (Morcrette 1991).

Further progress in modeling climatic processes at resolutions attainable in present-day GCMs probably will require a more fundamental understanding of the spatial and temporal scales implicit in different physical parameterizations so that model physics can be matched appropriately with gridscale dynamics. Theoretical work on such scale-matching problems will be necessary (e.g., Lindzen and Fox-Rabinowitz 1989), but much effort will also need to be invested in empirical investigations of these questions. In our view, advances on this front can be accelerated by carrying out systematic intercomparison studies that focus on specific aspects of climate modeling (e.g., Cess et al. 1990, Grotch and MacCracken 1991, Randall et al. 1992). In particular, a careful comparison of the effects of the full array of convection and cloud-formation schemes that are presently used in GCMs would be a worthwhile next step.

Acknowledgments. The cooperation of the staff of the European Centre for Medium Range Weather Forecasts in making their model available for this research and in offering helpful comments on an earlier draft of this paper is gratefully acknowledged. We relied upon major support from Robert Mobley, John Stout, Robert Drach, and Dean Williams for the modeling, data-access, and visualization aspects of the study. Interpolation and diagnostic routines that greatly expedited the analysis were kindly supplied by Peter Gleckler and Mary Meyer. Julia Slingo also gave valuable assistance in analyzing the impact of resolution on model clouds and in suggesting additional diagnostic approaches. This work was performed under the auspices of the U.S. Department of Energy, Environmental Sciences Division, by the Lawrence Livermore National Laboratory under Contract W-7405-ENG-48.

REFERENCES

Alexander, R.C., and R.L. Mobley, 1976: Monthly average sea-surface temperatures and ice-pack limits on a 1 degree global grid, *Mon. Wea. Rev.*, **104**, 143-148.

Battisti, D.S., P.G. Hess and P.J. Rasch, 1991: The maintenance of the intertropical convergence zones on a water covered Earth. Proceedings of the AMS Fifth Conference on Climatic Variations, 14-18 October 1991, Denver, CO, 222-225.

Blondin, C. and H. Böttger, 1987: The surface and sub-surface parameterization in the ECMWF forecasting system: Revision and operational assessment of weather elements. ECMWF Tech. Memo. No. 135, European Centre for Medium Range Weather Forecasts, Reading, England.

Boer, G.J., and M. Lazare, 1988: Some results concerning the effect of horizontal resolution and gravity-wave drag on simulated climate. *J. Climate*, **1**, 789-806.

Boer, G.J., K. Arpe, M. Blackburn, M. Deque, W.L. Gates, T.L. Hart, H. Le Treut, E. Roeckner, D.A. Sheinin, I. Simmonds, R.N.B. Smith, T. Tokioka, R.T. Wetherald and D. Williamson, 1991: An intercomparison of the climates simulated by 14 atmospheric general circulation models. World Climate Research Programme, Geneva, Switzerland, 37 pp.

Boville, B.A., 1991: Sensitivity of simulated climate to model resolution. *J. Climate*, **4**, 469-485.

Boyle, J.S., 1993: Sensitivity of dynamical quantities to horizontal resolution for a climate simulation using the ECMWF (cycle 33) model. PCMDI Report No. 6 and *J. Climate* (in press).

Cess, R.D, G.L. Potter, J.P. Blanchet, G.J. Boer, A.D. DelGenio, M. Deque, V. Dymnikov, V. Galin, W.L. Gates, S.J. Ghan, J.T. Kiehl, A.A. Lacis, H. Le Treut, Z.-X. Li, X.-Z. Liang, B.J. McAvaney, V.P. Meleshko, J.F.B. Mitchell, J.-J. Morcrette, D.A. Randall, L. Rikus, E. Roeckner, J.F. Royer, U. Schlese, D.A. Sheinin, A.

Slingo, A.P. Sokolov, K.E. Taylor, W.M. Washington, R.T. Wetherald, I. Yagai and M.-H. Zhang, 1990: Intercomparison and interpretation of climate feedback processes in 19 atmospheric general circulation models. *J. Geophys. Res.*, **95**, 16601-16615.

ECMWF Research Department, 1988a: ECMWF Forecast Model, Adiabatic Part (2nd edition). European Centre for Medium Range Weather Forecasts, Reading, England.

ECMWF Research Department, 1988b: ECMWF Forecast Model, Physical Parameterisation (2nd edition). European Centre for Medium Range Weather Forecasts, Reading, England.

Gleckler, P., and K.E. Taylor, 1993: The effect of horizontal resolution on ocean surface energy fluxes in the ECMWF model. PCMDI Report No. 3 and *Climate Dynamics* (in press).

Grotch, S.L., and M.C. MacCracken, 1991: The use of general circulation models to predict regional climatic change. *J. Climate*, **4**, 269-285.

Janowiak, J.E., 1992: Tropical rainfall: A comparison of satellite-derived rainfall estimates with model precipitation forecasts, climatolgies, and observations. *Mon. Wea. Rev.*, **120**, 448-462.

Kiehl, J.T., and D.L. Williamson, 1991: Dependence of cloud amount on horizontal resolution in the NCAR Community Climate Model. *J. Geophys. Res.*, **96**, 10955-10980.

Kuo, H.L., 1974: Further studies of the parameterization of the influence of cumulus convection on large-scale flow. *J. Atmos. Sci.*, **31**, 1232-1240.

Laprise, R., 1992: The resolution of global spectral models. *Bull. Amer. Met. Soc.*, **73**, 1453-1454.

Legates, D.R., and C.J. Willmott, 1990: Mean seasonal and spatial variability in gauge-corrected, global precipitation. *Int. J. Climatol.*, **10**, 111-127.

Lindzen, R.S., and M. Fox-Rabinovitz, 1989: Consistent vertical and horizontal resolution, *Mon. Wea. Rev.*, **117**, 2575-2583.

Manabe, S., J. Smagorinsky, J.L. Holloway, and H.M. Stone, 1970: Simulated climatology of a general circulation model with a hydrologic cycle. III: Effects of increased horizontal computational resolution. *Mon. Wea. Rev.*, **98**, 175-212.

Miller, M.J., T.N. Palmer and R. Swinbank, 1989: Parameterization and influence of subgridscale orography in general circulation and numerical weather prediction models. *Meteor. Atmos. Phys.*, **40**, 84-109.

Miller, M.J., A.C.M. Beljaars and T.N. Palmer, 1992: The sensitivity of the ECMWF model to the parameterization of evaporation from the tropical oceans. *J. Climate*, **5**, 418-434.

Morcrette, J.-J.,1989: Description of the radiation scheme in the ECMWF model. ECMWF Tech. Memo. No. 165. European Centre for Medium Range Weather Forecasts, Reading, England26 pp.

Morcrette, J.-J., 1991: Cloud and radiation fields in the ECMWF model: Dependence of model horizontal resolution and representation of moist processes. IAMAP Program and Abstracts, XX General Assembly of the IUGG, 11-24 August 1991, Vienna, Austria, p. 66.

Potter, G.L., J.S. Boyle, K.R. Sperber and S. Hameed, 1993: Effect of spatial resolution on the simulation of regional precipitation in China in a global climate model. Proceedings of the AMS Fourth Conference on Global Change Studies, 17-22 January 1993, Anaheim, CA.

Randall, D. A., R. D. Cess, J. P. Blanchet, G. Boer, A. D. DelGenio, M. Deque, V. Dymnikov, V. Galin, W. L. Gates, S. J. Ghan, J. T. Kiehl, A. A. Lacis, H. Le Treut, Z.-

X. Li, X.-S. Liang, B. J. McAvaney, V. P. Meleshko, J. F. B. Mitchell, J. J. Morcrette, G. L. Potter, L. Rikus, E. Roeckner, J. F. Royer, U. Schlese, D. A. Sheinin, A. Slingo, A. P. Sokolov, K. E. Taylor, W. M. Washington, R. T. Wetherald, I. Yagai and M.H. Zhang, 1992: Intercomparison and interpretation of surface energy fluxes in atmospheric general circulation models., *J. Geophys. Res.*, **97**, 3711-3724

Rao, D.V.B., K. Yamazaki and A. Kitoh, 1991: Some GCM experiments of the Asian summer monsoon related to land boundary conditions. *Papers in Meteor. Geophys.*, **42**, 127-143.

Rind, D., 1988: Dependence of warm and cold climate depiction on climate model resolution. *J. Climate*, **1**, 965-997.

Roads, J., S-C. Chen, J. Kao, D. Langley and G. Glatzmaier, 1992: Global aspects of the Los Alamos general circulation model hydrologic cycle. *J. Geophys. Res.*, **97**, 1051-1068.

Simmons, A.J., D.M. Burridge, M. Jarraud, C. Girard and W. Wergen, 1989: The ECMWF medium-range prediction models, development of the numerical formulations, and the impact of increased resolution. *Met. Atmos. Physics*, **40**, 28-60.

Slingo, J., 1987: The development and verification of a cloud prediction model for the ECMWF model. *Quart. J. Roy. Met. Soc.*, **113**, 899-927.

Sperber, K.R., 1993: The effect of horizontal resolution on the simulation of the Indian monsoon in the ECMWF model. PCMDI Report (in preparation), Program for Climate Model Diagnosis and Intercomparison, Lawrence Livermore National Laboratory, Livermore, CA.

Stephens, G.L., 1990: On the relationship between water vapor over the oceans and sea surface temperature. *J. Climate*, **3**, 634-645.

Sundqvist, H., 1978: A parameterization scheme for non-convective condensation including prediction of cloud water content. *Quart. J. Roy. Met. Soc.*,**104**, 677-690.

Tibaldi, S., T.N. Palmer, C. Brankovic and U. Cubasch, 1990: Extended-range predictions with ECMWF models: Influence of horizontal resolution on systematic error and forecast skill. *Quart. J. Roy. Met. Soc.*, **116**, 835-866.

Tiedtke, M., 1989: A comprehensive mass flux scheme for cumulus parameterization in large-scale models. *Mon. Wea. Rev.*, **117**, 1779-1800.

Wellck, R.E., A. Kasahara, W.M. Washington and G.D. Santo, 1971: Effect of horizontal resolution in a finite-difference model of the general circulation. *Mon. Wea. Rev.*, **99**, 673-683.